Understanding the perovskite/self-assembled selective contact interface for ultra-stable p-i-n and high efficient perovskite solar cells.

Ece Aktas,[Ŧ,1,2] Nga Phung,[Ŧ,3,#] Hans Köbler,[3] Dora A. González,[1,4] Maria Méndez,[1] Ivona Kafedjiska,[5] Silver Hamill Turren-Cruz,[3] Robert Wenisch,[5] Iver Lauermann,[5] Antonio Abate,[3,6] and Emilio Palomares*,[1,7]*

[1]Institute of Chemical Research of Catalonia (ICIQ-BIST). Avda. Països Catalans, 16. Tarragona. E-43007. Spain.

[2]Departament de Química-Física i Inorgànica. URV. E-43007. Spain.

[3]Helmholtz-Zentrum Berlin für Materialien und Energie GmbH, Kekuléstr. 5, Berlin D-12489, Germany.

[4]Departament d'Enginyeria Electrònica, Elèctrica i Automàtica. URV. Tarragona. E-43007. Spain.

[5]PVcomB/Helmholtz-Zentrum Berlin für Materialen und Energie, Schwarzschildstraße 3,12489 Berlin, Germany.

[6]Department of Chemical, Materials and Production Engineering, University of Naples Federico II, Piazzale Tecchio 80, 80125 Fuorigrotta, Italy.

[7]ICREA. Passeig LLuís Companys 23. E-08010. Spain.

[Ŧ]Both authors contributed equally to this work.

[#]Present address: Department of Applied Physics, Eindhoven University of Technology, 5600 MB Eindhoven, the Netherlands.

Email of corresponding authors:

antonio.abate@helmholtz-berlin.de

antonio.abate@unina.it

epalomares@ICIQ.es

Abstract

Current perovskite solar cell efficiency is close to silicon record values. Yet, the roadblock for industrialization of this technology is its stability. The stability of the solar cell not only depends on the stability of the perovskite material itself but also notably on its contact layers and their interface with the perovskite, which plays a paramount role. This study rationalizes the design of new molecules to form self-assembled monolayers as hole-selective contact. The new molecules increased the stability of perovskite solar cells to maintain 80% of its initial PCE of 21% for 250 h at 85 °C under 1 sun illumination. The excellent charge collection property as well as a perovskite passivation effect enable the highly stable and efficient devices demonstrating the vast potential of this new type of contacts in photovoltaic application.

Introduction

In a short 10 years learning curve, perovskite solar cell (PSCs) efficiency reached over 25% from an initial 3.8%.[1] Through all this process, the past knowledge in dye-sensitized solar cells and organic solar cells has been vital for rapid success. Moreover, charge selective contact layers become critical for having such high efficiency. Yet, despite having extraordinary progress on the device's efficiency, halide perovskite's long-term stability is one of the main roadblocks towards its industrialization. To improve the device's stability, not only the intrinsic stability enhancement of halide perovskite is essential, but also the stability of the device contact layers plays a crucial role. Highly-priced organic charge selective materials drive the research to look for new organic conjugated molecules like self-assembled monolayers (SAMs), which have been applied before in organic-based optoelectronic devices. Recently, SAMs have been used as charge selective contacts for PSCs and record power conversion efficiency has rapidly achieved to 21% under standard measurement conditions.[2–4]

Unlike organic hole selective materials whose prices are high (*e.g.* PTAA coasting 1000 euros per gram) or being unstable in devices,[5] SAMs offer an opportunity for a cheap, scalable, and stable hole-selective material in p-i-n type PSCs structure due to low concentration, simple processing, no required doping process, applicable for large scale deposition and modifiable bandgap. In addition to these advantages, SAMs can modulate the work function of the metal oxide surface for better control of the energy band alignment between the different materials and interfaces within the solar cell. This modulation can be achieved via SAMs' anchor groups such as carboxylic acid or phosphonic acid that can react with the surface hydroxyl groups of metal oxides by a simple chemical reaction.[6,7] Their functional groups are designed to modify the interface or surface properties like wetting, functionalities and, as mentioned above, the interfacial energy level alignment.[8–10] The linkage group is positioned between the anchoring group and functional group, which determines the packing geometries.

In this study, we designed and synthesized two new carbazole based self-assembled molecules for hole-selective layers (HSLs) in p-i-n solar cells. The two molecules have demonstrated stable efficiency above 21% delivering a solar cell open-circuit voltage (V_{OC}) of 1.19 V for a perovskite bandgap of 1.63 eV. Remarkably, solar

cells retain 80% of its initial conversion efficiency after 250 h maximum power point tracking under one sun AM 1.5 G illumination at 85 °C. These results are a new milestone for the development of a new class of hole selective materials in PSCs, which exhibits at the same time high efficiency and stability, which is paramount for the necessary transfer to industrial applications.

Result and Discussion

Molecule design and characterization

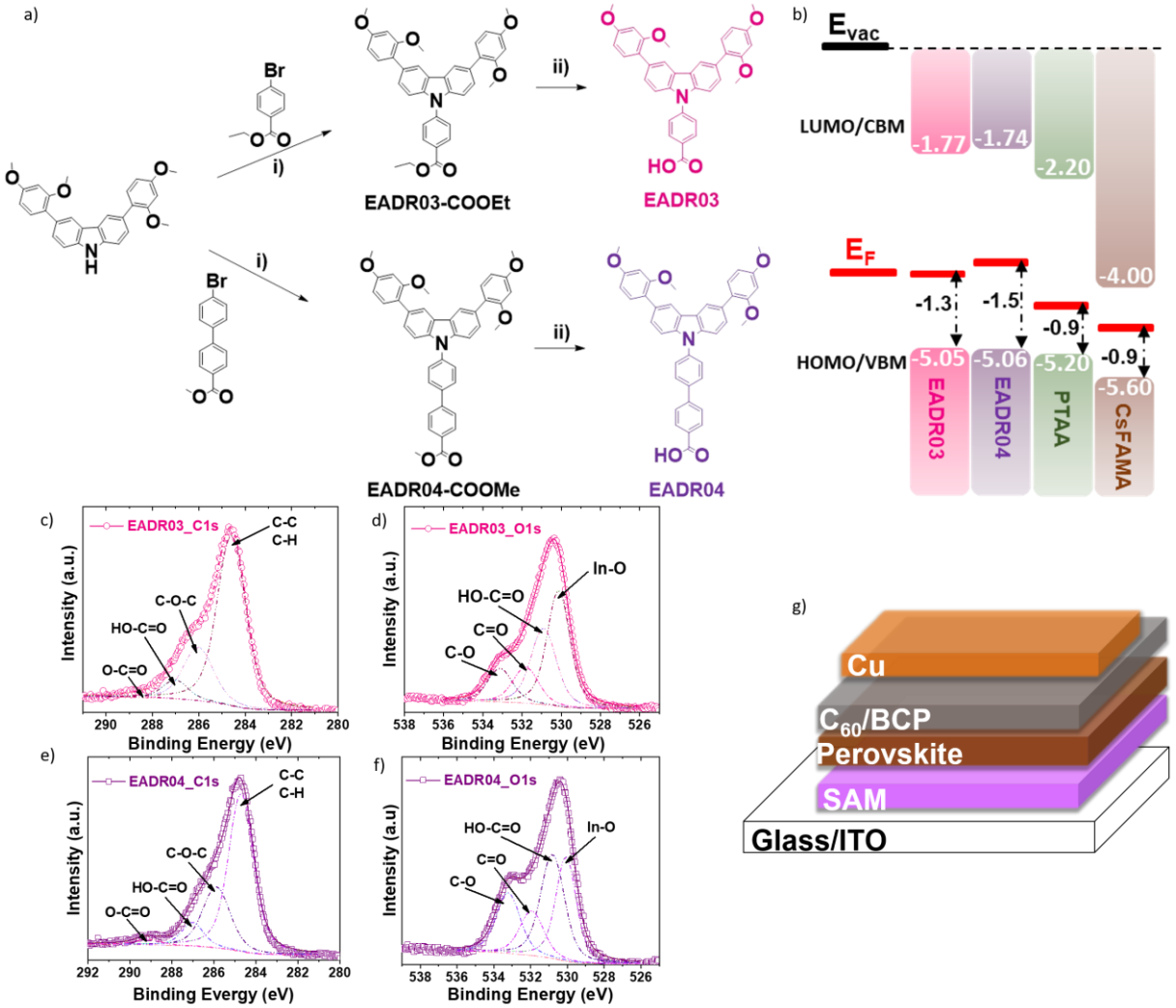

Figure 1. *a) Synthesis pathway of SAMs; i) Tris(dibenzylideneacetone)dipalladium(0) (0.10 equiv.), tri-tert-butylphosphine tetrafluoroborate (0.20 equiv.), sodium tert-butoxide (1.1 equiv.), dry Toluene (10.0 mL), Argon, 115 °C, 24 h ii) potassium hydroxide (10 equiv.), solvent mixture of methanol: tetrahydrofuran (1:1, v:v), 85 °C, 24 h. b) Energy alignment of different layers. The band edge positions of SAMs, PTAA and CsFAMA layer's from UPS measurements in the schematic representation. Note that the SAM layer's values (EADR03 and EADR04) are measured with UPS (Fig. S8 showed UPS spectra) (see Methods for detail). Before UPS measurement, the ITO substrate is treated with UV-Ozone to ensure similarity with used substrates in devices. c) The XPS high-resolution survey spectra of c) C1s d) O1s for ITO/EADR03 and e) C1s, f) O1s for ITO/EADR04. g) Schematic representation of the used p–i–n device structure.*

Fig. 1a shows the synthesis pathway of the new SAMs, where 4-(3,6-bis(2,4-dimethoxyphenyl)-9*H*-carbazol-9-yl)benzoic acid **(EADR03)** and 4'-(3,6-bis(2,4-dimethoxyphenyl)-9*H*-carbazol-9-yl)-[1,1'-biphenyl]-4-carboxylic acid **(EADR04)** have

a carbazole moiety as electron donor unit.[11] On the one hand, such a carbazole chemical group has electron-rich block properties, which leads to increase power conversion efficiencies (PCE) up to 18% in PSCs.[12–14] Subsequent electron-rich groups are mainly added as substituents in the carbazole moiety to align the energy levels with the perovskite material and increase its solubility in common organic solvents. On the other hand, the substituted position for the photo-active conjugated phenyl benzene plays a critical role in the electron-donating effect. For instance, if the methoxy groups are only located at the *meta*-position, it will have an electron-withdrawing effect.[15] Nevertheless, if it is only positioned at the *ortho*-position, it will twist the phenyl ring out of the plane, causing the undesired steric effect.[16] For those reasons, the 1,3-dimethoxybenzene is chosen as a substituent for carbazole moiety. The synthetic details are given in the ESI†.

To prove the suitable energetic properties as hole selective material for PSCs, we performed ultra-violet photoelectron spectroscopy (UPS) on SAM layer attached to indium-tin-oxide (ITO) substrate similar to what is used in the device. Here, ITO coated glasses are homogenously covered with SAMs by dipping method. The condensation reaction occurs between the carboxylic acid (-COOH) anchor group of SAMs and the surface hydroxyl group (-OH) of metal oxide to give ester (O-C=O) type linkages,[6,17] which result in the formation of a monolayer of SAM on the ITO. The bandgap of SAMs is estimated from the absorption edge wavelength ($\lambda_{a.e.}$) using UV-vis measurement[18] (see Fig. S3 and Table S2, ESI†) to calculate the position of the SAM's lowest unoccupied molecular orbital (LUMO). The valence band onset and the Fermi level value EADR03 and EADR04 are schematically displayed in Fig. 1b. In this study, we employed the triple cation perovskite ($Cs_{0.05}FA_{0.79}MA_{0.16}Pb(I_{0.84}Br_{0.16})_3$ onwards labelled as CsFAMA) as the absorber layer adapted from Saliba *et al.*[19] The energetic properties of PTAA and CsFAMA are obtained from the literature and all values reference to the vacuum level.[3] As can be seen from Fig. 1b, SAMs exhibits better electron blocking character than PTAA due to the carbazole unit in small molecule backbone while works as efficient hole extraction layers.

Additionally, as shown in Fig. 1a, we designed the SAM molecules with 1,3-dimethoxybenzene moiety acting as a terminal group that provides a miscible interface for the perovskite one-step solution process. A miscible interface ensures a homogenous and compact perovskite film.[20] To determine the surface wettability,

contact angle measurements are performed on bare ITO and p-type materials deposited on ITO (see the Method section for details). The contacting angles of the water on bare ITO, PTAA, EADR03 and EADR04 are 8.13˚, 88.15, 50.19˚ and 51.63, respectively (see Fig. S4, ESI†). PTAA layer shows a higher hydrophobicity than the SAMs in agreement with the previous report,[21] leading to a poor wetting for perovskite solution on PTAA. We note that in the XRD patterns (see Fig. S9, ESI†), though there is no detectable peak shift or peak broadening in the perovskite phase, however, there is a noticeable more pronounced PbI_2 phase in the perovskite on PTAA than on SAMs. This higher PbI_2 content is also visible in the SEM images as bright small grain on the surface (see Fig. S10, ESI†). Although it has been reported that excess PbI_2 in the perovskite can improve the device performance, a recent report has shown that higher PbI_2 consisted perovskite can lead to lower stability in devices due to the formation of metallic Pb, which can be non-radiative recombination centers.[22] Hence, together with degraded PTAA, the lower PTAA based device stability can be also attributed to the higher initial PbI_2 content of the film. However, this cannot explain the difference in device efficiency seen below because PbI_2 has been shown to be beneficial for improving V_{OC} in devices,[23] which implies that the superior device performance of SAMs is due to the excellent SAM electronic properties.

We examined the atomic bonds of SAMs on metal oxide surface using X-ray photoelectron spectroscopy (XPS). The spectra were analyzed as described in the supporting information (see Table S3, ESI†). The C1s spectra, were decomposed into 4 peaks assigned to C-C or C-H at 284.6 eV (284.7 eV), to C-O at 286.0 eV (285.9 eV), COOCH bonds at 287.0 eV (287.0 eV), and to O-C=O bonds at 288.5 eV (289.1 eV) for EADR03 (EADR04) (Fig. 1c and e respectively).[24,25] The [C-O] / [C-C + C-O] area ratios amount to 25% for EADR03 and 30% for EADR04. From the structure formulae, one would expect 15% for EADR03 and 12% for EADR04 ignoring attenuation due to inelastic electron scattering. The evident excess in C-O bonds is likely caused by solvent residues. It is worth noting that the bare ITO surface also exhibits C1s peaks situated at 284.9 eV, 285.8 eV, 287.0 eV, and 289.1 eV (see Fig. S5a, ESI†). These carbon contributions are presumably largely residues from the cleaning procedure. The O1s region, Fig. 1d and f exhibit peaks belonging to In-O at 530.1 eV, to surface hydroxides at 530.9 eV (530.8 eV), to C=O at 532.8 eV (532.8 eV) and C-O at 533.1 eV (533.2 eV) for EADR03 (EADR04) in the O1s spectra.[26,27] The bare ITO substrate also showed four components: 530.3 eV (InSnO), 530.8 eV, 531.8 eV, and

532.9 eV (see Fig. S5b, ESI†), where the carbon compounds are again presumably cleaning residues.

The formation of ester bonds demonstrates bonding between the carbon atom of carboxylic acid and the oxygen atom of the hydroxyl group on ITO or to solvent residues.[28] Moreover, we observe a much weaker signal of this characteristic ester bond in C1s and O1s spectra of a bare ITO in these regions, which further points to the presence of SAMs on ITO (see Fig. S6, ESI†). The N1s spectra show the same peak position of *ca*. 400 eV for both SAMs, indicating the presence of the C-N bond in the structure (see Fig. S6c, ESI†). These are a strong hint to the presence of SAMs on the ITO substrate.

To understand the charge transfer property of these new SAMs as HSLs for PSCs, we performed time-resolved photoluminescence (TRPL) using λ=470nm as excitation wavelength as shown in Figure S11. The traces exhibit two different decay profiles fitted to a bi-exponential function as previously reported.[29–31] SAM-based perovskite films show initial fast decay that can be assigned to trap filling, while the slower decay most likely corresponds to the bimolecular recombination. The lifetimes τ_1 of EADR03, EADR04, PTAA and the perovskite are 15 ns, 9 ns, 2 ns and 7 ns, respectively, and the lifetimes τ_2 calculated are 158 ns, 106 ns, 12 ns and 83 ns for EADR03, EADR04, PTAA and the perovskite, respectively (see Table S4, ESI†). Interestingly, in Fig. S11b (ESI†), the luminescence decay of perovskite layers on SAMs shows efficient quenching that supports their efficient hole transporting character compared to PTAA. Not only that we have evidence of a faster charge extraction using SAM compared to PTAA, but the increased PL yield can also indicate interfacial passivation effect[32] compared to PTAA sample shown in Fig. S11c (ESI†) similar to reported carbazole based polymer.[33]

Photovoltaic performance

We employed in this study the state-of-the-art device architecture with ITO/ SAM or PTAA/CsFAMA/C_{60}/BCP/Cu sandwich architecture in Fig. 1g.[34] Cesium-containing triple cation perovskite (CsFAMA) is deposited on top of the HSLs using the one-step method. Afterwards, C_{60}, an electron selective layer, is thermally evaporated on top of the perovskite layer. The fullerene C_{60} has excellent electron-extraction properties in photovoltaic devices. Thus it is preferred for the electron transport layer.[35] Lastly, a bathocuproine (BCP) and copper (Cu) electrode are evaporated to complete the device. SAMs are generally deposited on metal oxide surface as a monolayer through a variety of methods like solution assisted self-assembly (dipping), vapour deposition and spin-coating method.[27] Here, we used the paradigmatic PTAA as our baseline to determine the performance of cells with SAMs. PTAA is not only widely used in p-i-n PSCs as polymeric HSL, which can be coated into a thin homogenous layer from solution and show higher than 18% PCEs.[5,36,37] Detailed fabrication process of perovskite solar cells is presented in the Methods section of SI.

The choice of solvent is the first step and critical step for SAMs to have a well-organized interface between SAMs and perovskite absorber. Here the design of EADR03 and EADR04 consists of carboxylic acid moiety on the molecule backbone that is helpful to solve them in non-halogenated solvents as ethanol (EtOH) and isopropanol (IPA). The devices with SAMs as HSLs show statistically better performance with IPA using the dipping method compared to ethanol (see Fig. S12 and Fig. S13, ESI†). The best PV parameters of solvent optimization are summarized in Table S5. Consequently, we achieve more than 20% PCE with dipping method with EADR03 as the HSL, whereas spin coating method only has a maximum of 17% (see Fig. S14 and Fig. S15, ESI†). The best device parameters of EADR03 with different deposition methods are shown in Table S6 (ESI†). On the other hand, EADR04 is not suitable for spin-coating methods because of solubility problems. We note that here the dipping method is preferable due to lower solubility of the molecules in alcohol. Nonetheless, the solubility is not the only deciding factor for device performance. The molecules have excellent solubility in toluene, yet the devices using this solvent exhibit unsatisfactory performance (Table S5, ESI†). The reason behind the different behavior is beyond the scope of this study and will require further research.

Fig. 2b shows the current density *versus* voltage (J-V) scans of the best devices with PTAA, EADR03 and EADR04 measured at a scan rate of 100 mV/s from forward (V_{OC} to J_{SC}) to reverse bias. Maximum power point (MPP) tracks of the best devices are placed in Fig. 2b. MPP-tracked efficiencies are comparable with the respective J-V values, which is expected from the negligible hysteresis. A statistical distribution of the cell parameters is achieved from more than 15 devices for each HSLs in Fig. 2a showing systematically higher performance of SAM based cells compared to PTAA. The best PCE of EADR03 and EADR04 is 20.5% and 20.6% surpassing PTAA cells' best value of 18.9%. Remarkably, the V_{OC} values of SAM-based devices demonstrate more than 1.1 V and the fill factor (FF) values >80%. The superior electron blocking of SAM compared to PTAA is attributed to the higher V_{OC} and FF values of EADR03 and EADR04 compared to PTAA. Specifically, the voltage of SAM-based devices is approximately 150 mV larger than that of PTAA. This device performance improvement is not directly correlated to the HOMO level of the material as PTAA has a deeper HOMO level compared to SAMs (Fig. 1b): instead, SAM as a material, which can have *both* efficient charge transport and passivation effect, results in this improvement. We emphasize that we achieve this desirable property of a contact layer without the use of dopants, which has been shown to degrade the perovskite layer.[38] Our result resonates with the conclusion of Al-Ashouri *et al.*[3] on phosphonic anchor SAMs. These results establish the tremendous promising benefit of SAM as an attractive class of material for selective layers realized in both perovskite and organic PV.[2,39,40]

In addition, the J-V scan of SAM-HSL based full device showed a lower leakage current in place of PTAA under dark conditions in Fig. S18 (ESI†). Low dark current also indicates a high density of SAM on ITO. The integrated J_{SC} of the best devices from external quantum efficiency measurement (EQE) integration is shown in Fig. 2c. A higher current density is also thanks to less parasitic absorption of SAM compared to PTAA in the short wavelength range similar to phosphonic SAMs developed for the same device architecture.[41] Integrated J_{SC} values have a negligible difference (~1%) with the J_{SC} values gained from the J-V scans for the best device. The devices with the SAMs as HSLs show minor hysteresis index (HI)[42,43] between reverse and forward J-V scans. All photovoltaic parameters of the best devices are provided in Table 1.

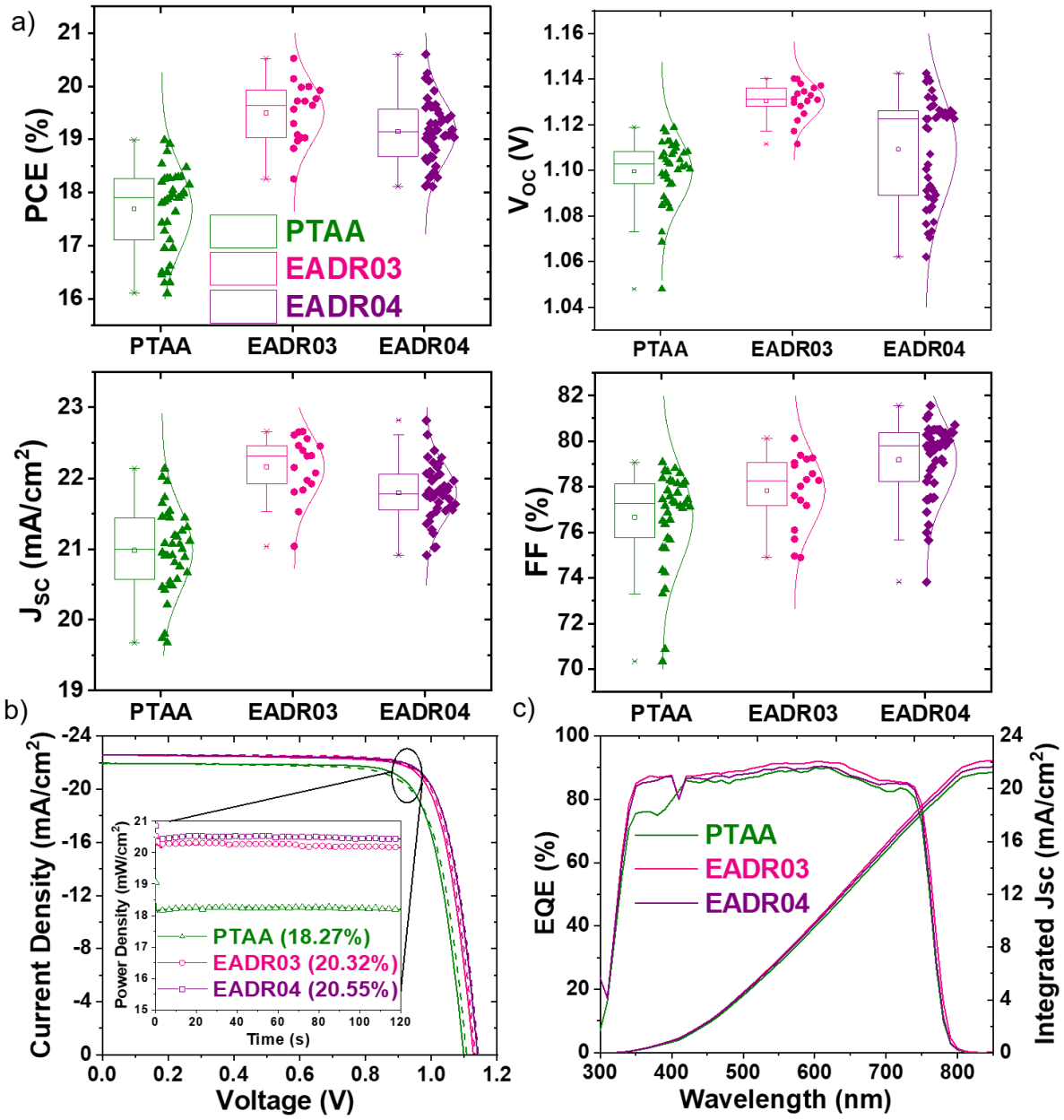

Figure 2*. a) Device performance statistic with different hole selective layers. b) Best J-V curves from PTAA, EADR03 and EADR04 with quasi-steady state efficiency. c) Corresponding external quantum efficiency curves which show integrated current density in agreement with values from J-V measurement.*

As we demonstrated the good passivation effect of SAM on the interface between perovskite and the HSLs compared to the commonly used polymer PTAA, the other interface with electron selective layer is equally important. It has been reported that the interfacial recombination at perovskite/C_{60} dominates the losses in voltage of this device architecture and it can be improved by an ultrathin passivation layer of LiF (~1nm).[34] In this study, we used the same approached to enhance further the final V_{OC} of the device, reaching 1.19 V with 1.63 eV bandgap perovskite with an

EADR03 based cell. Table 1 summarizes the champion devices in this study. As shown in Table 1, the improvement brought from LiF is higher in SAM-based devices compared to PTAA-based ones. This can be attributed to slightly higher PbI_2 content on the surface of the perovskite grown on PTAA than SAM (shown as bright grain in SEM images – Fig. S10, ESI†). The presence of PbI_2 on the surface can partially reduce the interfacial recombination at perovskite/C60 because of its wide bandgap.[44] With the improvement from LiF (V_{OC} enhanced for more than 50 mV) and an anti-reflection coating, the SAM-based device reached more than quasi-steady-state 21% for the EADR03 cell and 20.7% for EADR04 after 2 minutes of MPP tracking.

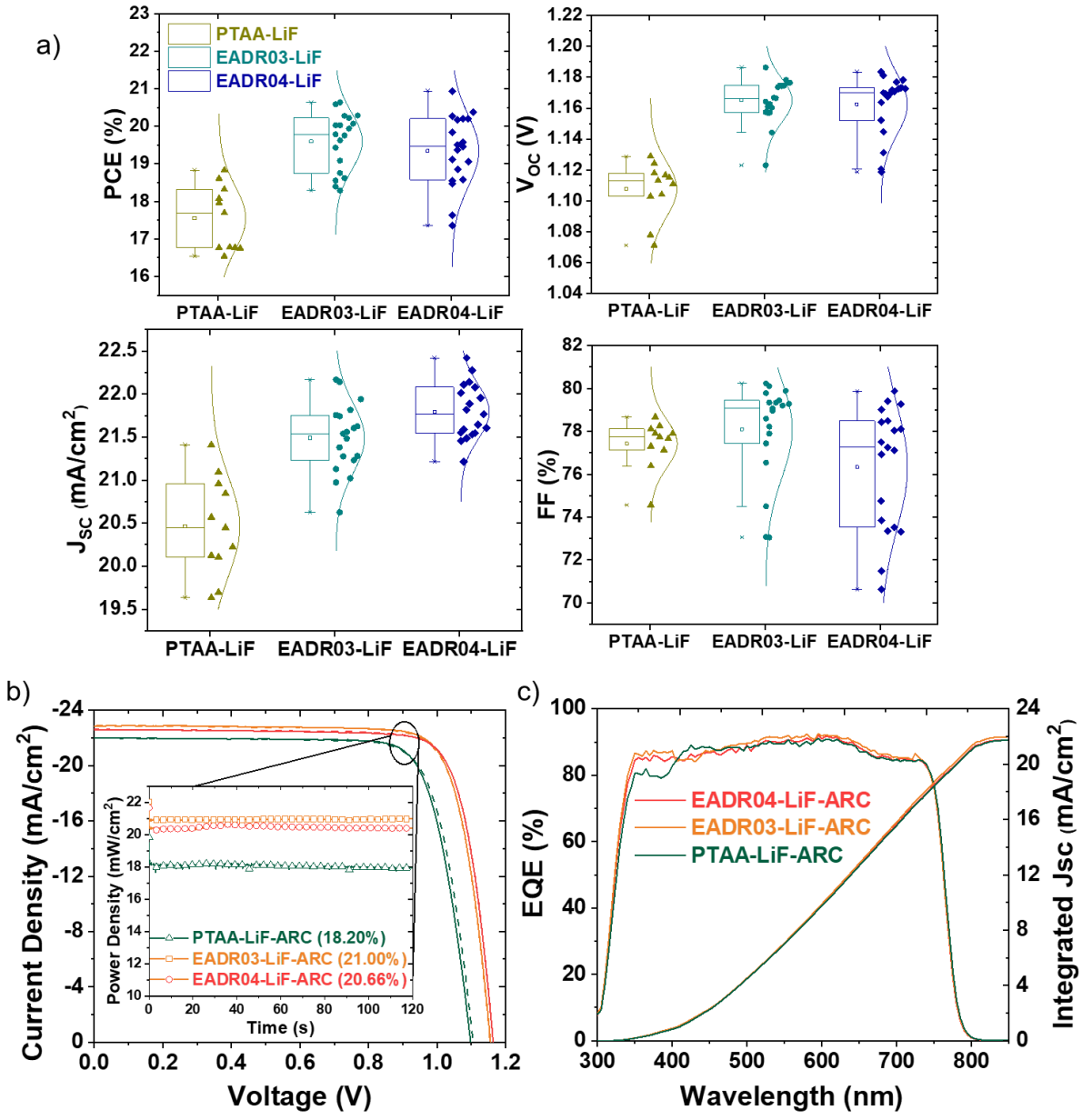

Figure 3. *a) Device performance statistic total of 50 devices from PTAA, EADR03 and EADR04 with LiF. b) Best J-V curves from PTAA, EADR03 and EADR04 with LiF and anti-reflection coating in the*

devices with quasi-steady state efficiency. c) Corresponding external quantum efficiency curves which show integrated current density in agreement with values from J-V measurement with anti-reflection coating.

Table 1. *Photovoltaic parameters of the best performing devices based on different HSLs with and without LiF and anti-reflection coating with a scan speed of 100 mV/s.*

HSLs	***LiF***	***ARC***	***Integrated J_{SC} (mA/cm^2)***	***J_{SC} (mA/cm^2)***	***V_{OC} (mV)***	***FF (%)***	***PCE (%)***	***HI (%)***
PTAA	No	No	21.2	21.9	1098	79	18.9	-0.01
PTAA	Yes	No	21.0	21.4	1124	78	18.8	0.06
PTAA	Yes	Yes	21.7	22.0	1105	78	18.9	0.00
EADR03	No	No	22.1	22.6	1132	80	20.5	0.00
EADR03	Yes	No	21.2	21.9	1186	79	20.5	0.03
EADR03	Yes	Yes	21.9	22.9	1156	80	21.2	0.00
EADR04	No	No	21.6	22.6	1140	80	20.6	-0.01
EADR04	Yes	No	21.0	22.2	1177	80	20.9	0.03
EADR04	Yes	Yes	21.8	22.6	1164	80	21.0	0.00

Device stability investigation

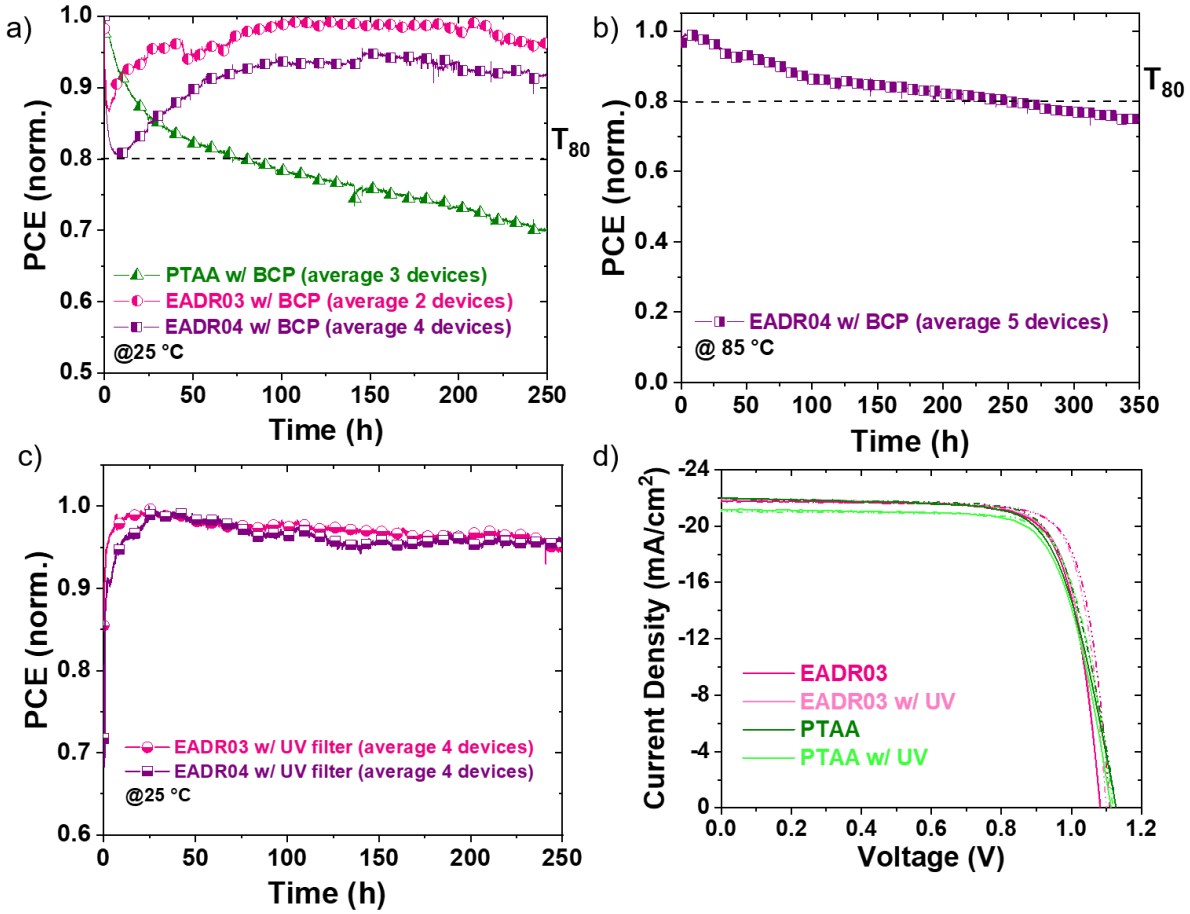

Figure 4. *Long-term continuous maximum power point tracking a) EADR03, EADR04 and PTAA based devices with BCP at 25 degree Celsius. b) EADR04 with BCP at 85 degree Celsius. c) EADR03 and EADR04 based devices with UV filter at 25 degree Celsius. Note that the values were averaged from different devices from different batches. All the measurements were done in an N_2 atmosphere without encapsulation. d) Best J-V curves from PTAA and EADR03 with and without UV light exposition (365 nm).*

Perovskite-based PV has reached 25.5% certified PCE and surpassed the conventional PV thin-film technologies and approaching the state-of-the-art silicon single-junction solar cell.[45] However, to integrate into the PV industry, perovskite's lack of stability is the main problem to tackle in the field.[46] Here, we use a high through-put ageing setup, which can track hundreds of devices at once. We compared the stability of PTAA with EADR03 and EADR04 cells in the continuous MPP in one sun illumination. As can be seen in Fig. 4a, the PTAA cells rapidly lost more than 15% of its initial PCE after 24 hours of MPP tracking. Meanwhile, the SAMs based devices exhibit outstanding higher stability (note that the curves are averaged from different devices and show statistical values rather than only best device).

The EADR04 cells, though showing a fast drop in the first few hours, regain its initial efficiency and retain 95% of the initial efficiency after 150 h of continuous MPP tracking before they have a declining trend. We extrapolate this trend and estimate the T_{80} (time until the cell reaches 80% of its initial efficiency) to result in a more than 800 hours T_{80} for EADR04 cells. Compared to EADR04 cells, the EADR03 cells gradually decrease until they reach 80% of initial PCE at around 180 h (as can also be seen in Table 2). This trend is more evident when the EADR04 cells are aged at an elevated temperature of 85 °C (see Fig. 4b) where the cells retain 80% of its initial efficiency after more than 240 h continuous MPP tracking. This difference between the two SAMs can be attributed to the structure of the molecules. As can be seen in Fig. S1 (ESI†), EADR04 has higher decomposition temperature compared to EADR03 thanks to extra phenyl in the linkage group (chain) between anchoring group and functional group. Note that the TGA indicates the decomposition temperatures (180 °C for EADR03 and 354 °C for EADR04), which is indeed not the same temperature as the operational conditions. However, TGA can still indicate the resiliency of the molecules in high temperature and long-time operation conditions. Similar to our observation, Li *et al.* has reported that different conjugated side-chain polymers results in devices with higher thermal stability.[47]

We attribute this encouraging improvement in the stability of SAMs as HSLs compared to PTAA to the excellent stability of SAMs in UV light. Indeed, when we exposed PTAA layers to the UV light for 30 minutes prior to perovskite deposition, the device exhibits lower J_{SC} whereas UV light has negligible effect on EADR03 (as can be seen in Fig. 4d). This negative impact on devices performance is more evidenced in the device statistic shown in Figure S19 (ESI†) where PTAA cells loss on average more than 1 mA/cm^2 after UV exposure. We emphasize that even without any UV light stress of the perovskite absorber layer, the UV has detrimental effect on PTAA in contrast of SAM whose devices did not show this behaviour.

The UV-induced degradation in PTAA is very likely due to the breaking of carbon bonds in the aromatic rings into smaller fragments.[48] In addition, polymers have been reported to undergo the photochemical pathway in which the polymer hydrocarbon chain can break down into free radicals in the presence of oxygen. This UV-photochemical can severely deteriorate polymeric material properties.[49] This also indicates a potential degradation pathway of polymer HSLs in ambient air that is undesirable for PSCs

application. We acknowledge that a bulk of PTAA (~ 10 nm) and a single molecular layer (1-3 nm) are compared in this study. The UV absorption of the SAM layer is negligible compared to the PTTA layer. We do expect that absorption of PTAA layer about 1 order of magnitude higher than SAM layer if we only consider the thicknesses of the two layers. Therefore, the defects that the UV absorption may create are more likely to impact the PTAA layer than the SAM layer. On the other side, an even thinner PTAA to have comparable thickness with SAM layers poses practical challenges. In fact, Stolterfoht *et al.* demonstrated that diluting PTAA solution led to having an incomplete coverage of ITO, decreasing the selectivity of the PTAA layer under the perovskite layer, which negatively affected devices' FF and V_{OC}.[50]

In this work, we have significantly higher intensity in the range of 300-500 nm with the used lamp for ageing measurements compared to global AM1.5 spectrum (see Fig. S20a, ESI†). Hence, the measurement condition accelerates the UV-induced PTAA degradation, which can be the reason behind the lower stability of our PTAA p-i-n cells compared to reported values in the literature (shown in Table 2). We note that high stability of PTAA in n-i-p cells has been reported,[51] nonetheless, in n-i-p structure, the UV photons are absorbed in the n-type and perovskite absorber layers before reaching PTAA. Moreover, this is also an accelerating ageing measurement for perovskite. The instability of perovskite under UV light has been widely reported,[52,53] mainly because of the photochemical degradation of PbI_2 into metallic lead Pb^0 forming non-radiative recombination centers, reducing the cells' efficiency.[22] We used a UV filter (cut-off at 350 nm) to improve the lifetime of the devices (see Fig. 4c). Although we still have a significantly higher intensity of the simulated spectrum in 350-500 nm region compared to global AM1.5 (see Fig. S21b, ESI†), we do see a considerable enhancement of the cells' lifetimes as can be seen in Table 2 (we note that the light intensity is lower than one sun illumination). The EADR04 cells' T_{80} reaches more than 2000 h. Therefore, the reported values in Table 2 are an underestimation of the cells' potential in this study.

Table 2. *Estimated T_{80} of the p-i-n perovskite solar cell with different HSLs from the MPP traces with and without UV filter.*

HSLs	Initial PCE (%)	Ageing Temperature and Illumination	Tracking Time (h)	Estimated T_{80} (h)

PTAA	18.5	25 °C, metal-halide lamp, 100 mW/cm^2	250	81
EADR03	19.3	25 °C, metal-halide lamp, 100 mW/cm^2	250	183
EADR03	19.9	25 °C, metal-halide lamp with UV filter, 100 mW/cm^2	250	1574
EADR04	17.9	25 °C, metal-halide lamp, 100 mW/cm^2	250	872
EADR04	19.9	25 °C, metal-halide lamp with UV filter, 100 mW/cm^2	250	2086
EADR04	20.1	85 °C, metal-halide lamp, 100 mW/cm^2	250	242
PTAA[*]	16	25 °C, White LED, 100 mW/cm^2	170	9,000

[*]The selected report has similar device architecture in inert gas conditions and room temperature.[37]

Conclusion

This study demonstrates the importance of the molecular design when using SAMs as selective contacts in perovskite solar cells. The SAMs have become the approach to achieve high solar-to-energy conversion efficiencies and, herein, we show that SAMs can lead to remarkable stable solar cells. In our study, we use both carbazole and methoxy moieties as electron donors for efficient charge selection, good electron blocking properties and surface passivation of the perovskite. Moreover, the 1,3-dimethoxybenzene terminal group of the molecule is compatible with perovskite formation resulting in a smooth and compact perovskite film. This design enables the perovskite cells reaching more than 21% stabilized efficiency and, most importantly, the monolayer based devices exhibit superior stability compared to PTAA based cells, which are the current standard for perovskite solar cells approaching silicon PV values. We demonstrated that stabilizing the perovskite/SAMs interface is the way to commercialize perovskite solar cells.

Acknowledgments

EA, DR, MM, and EP thank MINECO (projects CTQ2013-47183, CTQ 2017-89814-P, and CTQ2017-85393-P) and SGR-AGAUR 2017SGR00978. EP is also thankful to ICIQ and ICREA for economical support. This result is part of a project that has received funding from the European Research Council (ERC) under the European Union's Horizon 2020 research and innovation programme grant agreement No. number 804519. IK, IL, and RW acknowledge financial support by the German Federal Ministry for Economic Affairs and Energy in the frame of the speedCIGS project. EA thanks ICIQ for funding the internship in HZB. The authors thank Carola Klimm for taking SEM microscopic images. EA thanks Dr. Natalia Maticiuc for supporting XPS and UPS data analysis. NP thanks Amran Al-Ashouri for optimizing the device fabrication processes.

Author contributions

EA and NP conceived the idea, formulated the project and wrote the first draft of the manuscript under the supervision of EP and AA. EA and DR synthesized EADR03 and EADR04. EA and NP fabricated the devices and carried out the photo-physical characterization. HK and SHT carried out the Maximum Power Point Tracking studies of the devices. MM carried out Time-Correlated Single Photon Counting Measurements. RW and IK carried out X-ray Photoelectron Spectroscopy and Ultra-violet Photoelectron measurements under the supervision of IL. All authors participated in the discussion of the results and the manuscript writing and, finally, approved the submission.

References

1. Akihiro Kojima, Teshima, K., Shirai, Y. & Miyasaka, T. Organometal Halide Perovskites as Visible- Light Sensitizers for Photovoltaic Cells. *J. Am. Chem. Soc.* **131**, 6050–6051 (2009).

2. Yalcin, E. *et al.* Semiconductor self-assembled monolayers as selective contacts for efficient PiN perovskite solar cells. *Energy Environ. Sci.* **12**, 230–237 (2019).

3. Al-Ashouri, A. *et al.* Conformal monolayer contacts with lossless interfaces for perovskite single junction and monolithic tandem solar cells. *Energy Environ. Sci.* **12**, 3356–3369 (2019).

4. Li, L. *et al.* Self-assembled naphthalimide derivatives as an efficient and low-cost electron extraction layer for n-i-p perovskite solar cells. *Chem. Commun.* **55**, 13239–13242 (2019).

5. Yang, T. Y. *et al.* Achieving Long-Term Operational Stability of Perovskite Solar Cells with a Stabilized Efficiency Exceeding 20% after 1000 h. *Adv. Sci.* **6**, 1–7 (2019).

6. Brennan, B. J. *et al.* Comparison of silatrane, phosphonic acid, and carboxylic acid functional groups for attachment of porphyrin sensitizers to TiO2 in photoelectrochemical cells. *Phys. Chem. Chem. Phys.* **15**, 16605–16614 (2013).

7. Qiao, R. & Zuo, L. Self-assembly monolayers boosting organic-inorganic halide perovskite solar cell performance. *J. Mater. Res.* **33**, 387–400 (2018).

8. Love, J. C., Estroff, L. A., Kriebel, J. K., Nuzzo, R. G. & Whitesides, G. M. Self-Assembled Monolayers of Thiolates on Metals as a Form of Nanotechnology. *Chem. Rev.* **105**, 1103–1170 (2005).

9. Wojciechowski, K. *et al.* Heterojunction modification for highly efficient organic-inorganic perovskite solar cells. *ACS Nano* **8**, 12701–12709 (2014).

10. Casalini, S., Bortolotti, C. A., Leonardi, F. & Biscarini, F. Self-assembled monolayers in organic electronics. *Chem. Soc. Rev.* **46**, 40–71 (2017).

11. Zhu, X. *et al.* Hole-Transporting Materials Incorporating Carbazole into Spiro-Core for Highly Efficient Perovskite Solar Cells. *Adv. Funct. Mater.* **29**, 1807094 (2018).

12. Lu, C., Choi, I. T., Kim, J. & Kim, H. K. Simple synthesis and molecular engineering of low-cost and star-shaped carbazole-based hole transporting materials for highly efficient perovskite solar cells. *J. Mater. Chem. A* **5**, 20263–20276 (2017).

13. Yin, X. *et al.* One-step facile synthesis of a simple carbazole-cored hole transport material for high-performance perovskite solar cells. *Nano Energy* **40**, 163–169 (2017).

14. Rodríguez-Seco, C. *et al.* Minimization of Carrier Losses for Efficient Perovskite Solar Cells through Structural Modification of Triphenylamine Derivatives. *Angew. Chemie* **132**, 5341–5345 (2020).

15. Jeon, N. J. *et al.* o -Methoxy Substituents in Spiro-OMeTAD for Efficient Inorganic–Organic Hybrid Perovskite Solar Cells. *J. Am. Chem. Soc.* **136**, 7837–7840 (2014).

16. Krishna, A. & Grimsdale, A. C. Hole transporting materials for mesoscopic perovskite solar cells – towards a rational design? *J. Mater. Chem. A* **5**, 16446–16466 (2017).

17. Nazeeruddin, M. K., Humphry-Baker, R., Liska, P. & Grätzel, M. Investigation of Sensitizer Adsorption and the Influence of Protons on Current and Voltage of a Dye-Sensitized Nanocrystalline TiO 2 Solar Cell. *J. Phys. Chem. B* **107**, 8981–8987 (2003).

18. Costa, J. C. S., Taveira, R. J. S., Lima, C. F. R. A. C., Mendes, A. & Santos, L. M. N. B. F. Optical band gaps of organic semiconductor materials. *Opt. Mater. (Amst).* **58**, 51–60 (2016).

19. Saliba, M. *et al.* Cesium-containing triple cation perovskite solar cells: Improved stability, reproducibility and high efficiency. *Energy Environ. Sci.* **9**, 1989–1997 (2016).

20. Zuo, L. *et al.* Enhanced Photovoltaic Performance of CH 3 NH 3 PbI 3 Perovskite Solar Cells through Interfacial Engineering Using Self-Assembling Monolayer. *J. Am. Chem. Soc.* **137**, 2674–2679 (2015).

21. Safari, Z. *et al.* Optimizing the interface between hole transporting material and nanocomposite for highly efficient perovskite solar cells. *Nanomaterials* **9**, 1627

(2019).

22. Roose, B., Dey, K., Chiang, Y.-H., Friend, R. H. & Stranks, S. D. A Critical Assessment of the Use of Excess Lead Iodide in Lead Halide Perovskite Solar Cells. *J. Phys. Chem. Lett.* (2020) doi:10.1021/acs.jpclett.0c01820.

23. Du, T. *et al.* Formation, location and beneficial role of PbI2 in lead halide perovskite solar cells. *Sustain. Energy Fuels* **1**, 119–126 (2017).

24. Tozlu, C. *et al.* Effect of TiO2 modification with amino-based self-assembled monolayer on inverted organic solar cell. *Appl. Surf. Sci.* **422**, 1129–1138 (2017).

25. Moulder, J. F., Stickle, W. F., Sobol, P. E. & Bomben, K. D. Handbook of X-ray Photoelectron Spectroscopy. *Chastain, Publ. by Perkin-Elmer Corp.* (1992).

26. Montagne, F., Polesel-Maris, J., Pugin, R. & Heinzelmann, H. Poly(N-isopropylacrylamide) thin films densely grafted onto gold surface: preparation, characterization, and dynamic AFM study of temperature-induced chain 'conformational changes. *Langmuir* **25**, 983–991 (2009).

27. Yan, C., Zharnikov, M., Gölzhäuser, A. & Grunze, M. Preparation and characterization of self-assembled monolayers on indium tin oxide. *Langmuir* **16**, 6208–6215 (2000).

28. Arkan, E. *et al.* Effect of functional groups of self assembled monolayer molecules on the performance of inverted perovskite solar cell. *Mater. Chem. Phys.* 123435 (2020) doi:10.1016/j.matchemphys.2020.123435.

29. Palomares, E. J. *et al.* Supramolecular Coordination of Pb2+ Defects in Hybrid Lead Halide Perovskite Films Using Truxene Derivatives as Lewis Base Interlayers. *ChemPhysChem* cphc.201900068 (2019) doi:10.1002/cphc.201900068.

30. Kim, J. *et al.* Excitation Density Dependent Photoluminescence Quenching and Charge Transfer Efficiencies in Hybrid Perovskite / Organic Semiconductor Bilayers. **1802474**, 1–11 (2018).

31. Wen, X. *et al.* Defect trapping states and charge carrier recombination in organic-inorganic halide perovskites. *J. Mater. Chem. C* **4**, 793–800 (2015).

32. Hutter, E. M., Kirchartz, T., Ehrler, B., Cahen, D. & von Hauff, E. Pitfalls and

prospects of optical spectroscopy to characterize perovskite-transport layer interfaces. *Appl. Phys. Lett.* **116**, 100501 (2020).

33. Okada, W., Suga, T., Oyaizu, K., Segawa, H. & Nishide, H. Perovskite/TiO2 Interface Passivation Using Poly(vinylcarbazole) and Fullerene for the Photovoltaic Conversion Efficiency of 21%. *ACS Appl. Energy Mater.* **2**, 2848–2853 (2019).

34. Stolterfoht, M. *et al.* Visualization and suppression of interfacial recombination for high-efficiency large-area pin perovskite solar cells. *Nat. Energy* **3**, 847–854 (2018).

35. Wojciechowski, K. *et al.* C60 as an Efficient n-Type Compact Layer in Perovskite Solar Cells. *J. Phys. Chem. Lett.* **6**, 2399–2405 (2015).

36. Saliba, M. *et al.* How to Make over 20% Efficient Perovskite Solar Cells in Regular (n–i–p) and Inverted (p–i–n) Architectures. *Chem. Mater.* **30**, 4193–4201 (2018).

37. Stolterfoht, M. *et al.* Approaching the fill factor Shockley–Queisser limit in stable, dopant-free triple cation perovskite solar cells. *Energy Environ. Sci.* **10**, 1530–1539 (2017).

38. Habisreutinger, S. N. *et al.* Enhanced Hole Extraction in Perovskite Solar Cells Through Carbon Nanotubes. *J. Phys. Chem. Lett.* **5**, 4207–4212 (2014).

39. Aktas, E., Jiménez-López, J., Azizi, K., Torres, T. & Palomares, E. Self-assembled Zn phthalocyanine as a robust p-type selective contact in perovskite solar cells. *Nanoscale Horizons* **5**, 1415–1419 (2020).

40. Lin, Y. *et al.* Self-Assembled Monolayer Enables Hole Transport Layer-Free Organic Solar Cells with 18% Efficiency and Improved Operational Stability. *ACS Energy Lett.* **5**, 2935–2944 (2020).

41. Magomedov, A. *et al.* Self-Assembled Hole Transporting Monolayer for Highly Efficient Perovskite Solar Cells. *Adv. Energy Mater.* **8**, 1801892 (2018).

42. Habisreutinger, S. N., Noel, N. K. & Snaith, H. J. Hysteresis Index: A Figure without Merit for Quantifying Hysteresis in Perovskite Solar Cells. *ACS Energy Lett.* **3**, 2472–2476 (2018).

43. Snaith, H. J. *et al.* Anomalous hysteresis in perovskite solar cells. *J. Phys. Chem. Lett.* **5**, 1511–1515 (2014).

44. Wang, L., McCleese, C., Kovalsky, A., Zhao, Y. & Burda, C. Femtosecond time-resolved transient absorption spectroscopy of CH 3NH3PbI3 perovskite films: Evidence for passivation effect of pbi2. *J. Am. Chem. Soc.* **136**, 12205–12208 (2014).

45. National Renewable Energy Laboratory. PV Efficiency Chart. (2020).

46. Wang, Q., Phung, N., Di Girolamo, D., Vivo, P. & Abate, A. Enhancement in lifespan of halide perovskite solar cells. *Energy Environ. Sci.* **12**, 865–886 (2019).

47. Li, Z. *et al.* Side-Chain Engineering for Enhancing the Thermal Stability of Polymer Solar Cells. *Adv. Mater.* **27**, 6999–7003 (2015).

48. Petrović, M. *et al.* Limitations of a polymer-based hole transporting layer for application in planar inverted perovskite solar cells. *Nanoscale Adv.* **1**, 3107–3118 (2019).

49. Gijsman, P., Meijers, G. & Vitarelli, G. Comparison of the UV-degradation chemistry of polypropylene, polyethylene, polyamide 6 and polybutylene terephthalate. *Polym. Degrad. Stab.* **65**, 433–441 (1999).

50. Stolterfoht, M. *et al.* Approaching the fill factor Shockley–Queisser limit in stable, dopant-free triple cation perovskite solar cells. *Energy Environ. Sci.* **10**, 1530–1539 (2017).

51. Saliba, M. *et al.* Incorporation of rubidium cations into perovskite solar cells improves photovoltaic performance. *Science (80-.).* **354**, 206–209 (2016).

52. Farooq, A. *et al.* Spectral Dependence of Degradation under Ultraviolet Light in Perovskite Solar Cells. *ACS Appl. Mater. Interfaces* **10**, 21985–21990 (2018).

53. Li, W. *et al.* Enhanced UV-light stability of planar heterojunction perovskite solar cells with caesium bromide interface modification. *Energy Environ. Sci.* **9**, 490–498 (2016).